Serendipitous discovery of quadruply imaged quasars: two diamonds

John R. Lucey,[1]★ Paul L. Schechter,[2] Russell J. Smith[1] and T. Anguita[3,4]

[1]*Centre for Extragalactic Astronomy, Department of Physics, Durham University, Durham DH1 3LE, UK*
[2]*MIT Kavli Institute, Cambridge, MA 02139, USA*
[3]*Departamento de Ciencias Fisicas, Universidad Andres Bello, Fernandez Concha 700, Las Condes, Santiago, Chile*
[4]*Millennium Institute of Astrophysics, Chile*

ABSTRACT

Gravitationally lensed quasars are powerful and versatile astrophysical tools, but they are challengingly rare. In particular, only $\sim$25 well-characterized quadruple systems are known to date. To refine the target catalogue for the forthcoming Taipan Galaxy Survey, the images of a large number of sources are being visually inspected in order to identify objects that are confused by a foreground star or galaxies that have a distinct multicomponent structure. An unexpected by-product of this work has been the serendipitous discovery of about a dozen galaxies that appear to be lensing quasars, i.e. pairs or quartets of foreground stellar objects in close proximity to the target source. Here, we report two diamond-shaped systems. Follow-up spectroscopy with the IMACS instrument on the 6.5m Magellan Baade telescope confirms one of these as a $z = 1.975$ quasar quadruply lensed by a double galaxy at $z = 0.293$. Photometry from publicly available survey images supports the conclusion that the other system is a highly sheared quadruply imaged quasar. In starting with objects thought to be galaxies, our lens finding technique complements the conventional approach of first identifying sources with quasar-like colours and subsequently finding evidence of lensing.

Key words: gravitational lensing: strong – quasars: individual: 2M1134–2103, 2M1310–1714.

1 INTRODUCTION

Lensed quasars are used for a variety of cosmological and astronomical applications (Refsdal 1964; Wambsganss, Paczynski & Katz 1991; Claeskens & Surdej 2002; Schechter & Wambsganss 2004; Treu & Marshall 2016), most of which are limited by the relatively small number of systems available. In particular, quadruply imaged systems provide more restrictive constraints on lensing models, but only $\sim$15 of these 'quads' are suitable for use in any given analysis (e.g. Blackburne et al. 2011; Schechter et al. 2014). Hence, the discovery of more lensed quasars, especially quad systems, is valuable for further progress in several fields.

As new imaging surveys are carried out they are scoured for lensed quasars, with recent discoveries including a quadruply imaged system identified by Agnello et al. (2017) from SDSS DR12 imaging (Abazajian et al. 2009); a quad and several doubles discovered by Schechter et al. (2017) from VST-ATLAS (Shanks et al. 2015); and another quad in the Pan-STARRS PS1 survey (Chambers et al. 2016), found by Berghea et al. (2017) and another found by Ostrovski et al. (2018).

Only a small fraction of galaxies harbour quasars, so it is far more likely that a randomly chosen quasar will have a foreground galaxy projected close to the line of sight than vice versa. As a result, most lensed quasar systems have been found by careful examination of objects first thought to be quasars. Only a handful of objects first identified as galaxies have subsequently been found to be lensed background quasars (Huchra et al. 1985; Johnson et al. 2003; McGreer et al. 2010).

With deeper surveys, however, galaxy–quasar lens systems are more likely to have the colours of galaxies than those of quasars. A cartoon of the argument proceeds as follows: all quasars are at redshift $\sim$2; all lensing galaxies are at redshift $\sim$0.5; image separation is governed by velocity dispersion in the lens, which in turn is strongly correlated with luminosity of the galaxy, so at fixed separation, deeper surveys will sample fainter quasars but not fainter galaxies. It follows that to find fainter lensed quasars one must look for objects that, to first approximation, appear to be galaxies. Broadening the argument to take into account the range of quasar and galaxy redshifts does not change this conclusion.

The Taipan Galaxy Survey (da Cunha et al. 2017) is a southern sky, multi-object fibre-based spectroscopic survey that will obtain redshifts for over 1.2 million galaxies ($J_{\rm Vega} < 15.4$, $i \leq 17$) and measure Fundamental Plane distances for over 50 000 early-type galaxies within $z < 0.1$. In order to refine the target selection, and

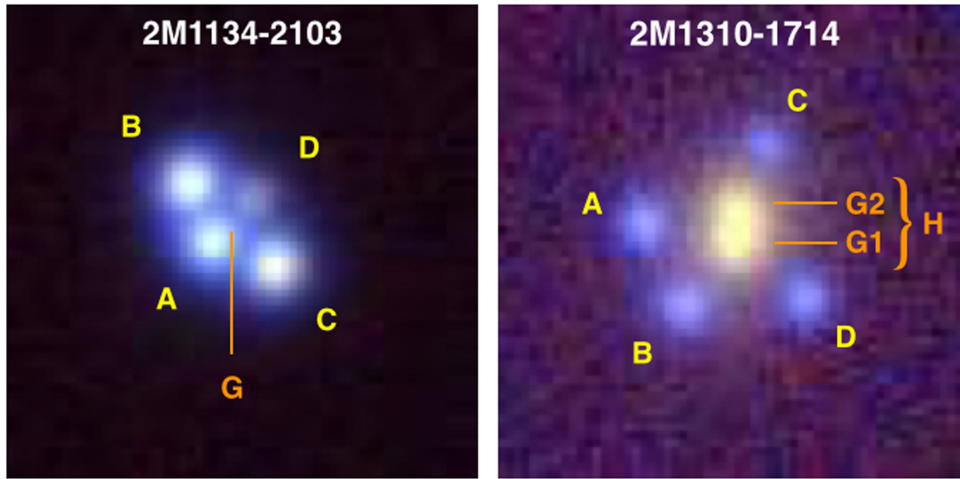**Figure 1.** PS1 image extracts (15×15 arcsec^2) of 2M1134–2103 (left) and 2M1310–1714 (right), constructed from *giy* data. Labels identify the quasar images *A–D* and the lensing galaxies. For 2M1134–2103, the lens is not seen in this image; for 2M1310–1714 we show schematically the two compact components (*G*1, *G*2) and one extended component (*H*) used to model the lens.

improve the efficiency of the survey, the lead author is visually examining the best available imaging data for the targets to identify sources that are confused by a foreground star or galaxies that have a distinct multicomponent structure. Initially, Pan-STARRS PS1 (Chambers et al. 2016) image data is being used for this endeavor. A by-product of this work has been the serendipitous discovery of about a dozen galaxies that appear to be lensing quasars, i.e. pairs or quartets of foreground stars in close proximity to (or masquerading as) the target galaxy.

Here, we report two diamond-shaped quad systems (see Fig. 1). While chance superpositions of galaxies and stars may occasionally mimic doubly imaged quasars, quadruply imaged quasars are much more difficult to mimic. For the simplest (monopole + quadrupole) lenses the positions of the images are very nearly confined to a five-dimensional subspace of an eight-dimensional configuration space (two positions for each of four images). A random distribution of four images in the neighbourhood of a galaxy almost never looks like a quadruply imaged quasar.

In Section 2, we describe the procedure that produced the candidate lenses. In Sections 3 and 4, we use FITS cutouts from ATLAS, Pan-STARRS PS1, and VISTA to produce astrometry and photometry for the quasar images and the lensing galaxies. In Section 5, we briefly discuss biases in the lensed quasar systems discovered and implications for future efforts.

2 REFINING THE TAIPAN TARGET CATALOGUE

The Taipan Phase-1 input catalogue is drawn from 2MASS (Skrutskie et al. 2006), selecting targets from the extended source catalogue (XSC; Jarrett et al. 2000) and supplemented with sources that are marginally resolved in the 2MASS point source catalogue (PSC; Cutri et al. 2003). Full details are given in Section 4.2.1 of da Cunha et al. (2017). 2MASS is a shallow survey and has a point-spread function (PSF) FWHM of ∼3.2 arcsec. We estimate that ∼5 per cent of the sources in the Taipan Phase-1 input catalogue are either confused by a foreground star or are multicomponent galaxy sources. In order to exclude from the sample these 'problem' sources, or to improve their astrometry for the fibre spectrocopy, all galaxies in the Taipan target catalogue are being visually inspected

using best available image sources. Initially, this work is concentrated on the objects for which PS1 imagery is available, i.e. those that are north of –30 deg Declination.

The visual inspection procedure is as follows. PS1 colour image cutouts of 1×1 arcmin^2 and PS1 photometric parameters of the Taipan targets ($n \sim 700\,000$) were collected. Targets drawn from the 2MASS PSC and XSC were examined separately, and were initially sub-divided into three categories: (i) objects where the difference between the PSF magnitude and the Kron magnitude, in the PS1 *i*-band, is less than 0.3 mag (these are mostly stars or galaxies with a brighter contaminating star), (ii) objects where the cross-matched PS1 and 2MASS positions differ by more than one arcsec, and (iii) the rest of the sample. To aid the visual inspection process, the GAIA DR1 sources were overlaid on the PS1 postage stamp images; this helps to identify contaminating stellar sources. About 50 per cent of 2MASS XSC sources have a GAIA DR1 counterpart. As of 2017 November, the lead author has inspected all ∼131 000 sources drawn from the 2MASS PSC and ∼120 000 objects drawn from the 2MASS XSC, of which ∼70 000 are in categories (i) and (ii).

This visual inspection of large numbers of relatively nearby bright ($J_{Vega} < 15.4$, $i \leq 17$) galaxies has lead to the serendipitous discovery of about a dozen galaxies that appear to be lensing quasars. The inspection process was not designed to discover lenses, and is on-going. Here, we report the two convincing quadruply imaged quasars that we have discovered so far.

3 2M1134–2103

At this location 2MASS PSC records a close pair of stellar objects, i.e. 2MASSJ11344050–2103230, 2MASS11344059–2103220. Their inclusion in the Taipan input catalogue results from their slightly extended nature and hence they were given a high priority in the visual inspection work. In the PS1 catalogue, this system is deblended into the three brightest components. We label this object hereafter as 2M1134–2103 (Fig. 1, left). At a galactic latitude of +38 deg, it is unlikely that four point sources of so nearly the same magnitude could be a chance superposition. Moreover, the symmetric image positions are characteristic of a 'core quad' lensing configuration (in the taxonomy of Saha & Williams 2003),

Table 1. Observed and modelled parameters of the 2M1134–2103 lens system. The positions Δx ($=\Delta\alpha\cos\delta$), Δy ($=\Delta\delta$) are in arcsec relative to quasar image A, and were derived from the VST ATLAS *i* band image. The magnitudes and colours are from PS1 (*griz*) and the VISTA Hemisphere Survey (JK_s). The final five columns provide the predicted position in our adopted lensing model (singular isothermal sphere plus external shear in this case), and the predicted magnification ratio (μ, with sign indicating image parity), the local convergence (κ) and the local shear (γ). The latter parameters are relevant for microlensing analyses. Observed image *G* refers to the residual peak seen in Fig. 2; the model position for *G* is the lens centre. Observed source *S* is the reference star.

Image	Δx	Δy	i_{PS}	$g-r$	$r-i$	$i-z$	K_s	$J-K_s$	Δx_{mod}	Δy_{mod}	μ_{mod}	κ_{mod}	γ_{mod}
A	0.00	0.00	16.94	0.27	0.13	−0.03	15.24	0.62	+0.020	+0.012	−1.51	0.58	0.92
B	+0.74	+1.75	16.96	0.31	0.27	0.00	15.29	0.60	+0.751	+1.746	+2.36	0.34	0.11
C	−1.93	−0.77	17.00	0.33	0.30	−0.01	15.44	0.52	−1.938	−0.753	+2.22	0.32	0.10
D	−1.23	+1.35	18.53	0.39	0.23	−0.01	16.83	0.61	−1.253	+1.327	−0.80	0.79	1.13
G	−0.74	+0.66					17.58	1.73	−0.752	+0.740			
S	−34.00	+3.10	16.43	0.45	0.20	0.06	14.99	0.41					

albeit with a 2 : 1 axis ratio which suggests a strong shear and/or ellipticity in the lensing potential.

3.1 Astrometry and photometry

We have not yet acquired spectroscopic confirmation of 2M1134–2103 as a lensed quasar system, but detailed inspection of the available optical and near-infrared imaging survey data provides further evidence in support of the lensing hypothesis.

We measure positions for the four components from the VST-ATLAS *i* image, using a program purpose-built to fit multiple PSFs and quasi-Gaussians[1] to lensed quasar systems. The low-level subroutines for this task are drawn from the DoPHOT photometry program (Schechter, Mateo & Saha 1993). While the PS1 images are deeper, the VST-ATLAS *i* image has better seeing (0.72 versus 1.08 arcsec). This is particularly important for astrometry of the four quasar components if the lensing galaxy contributes light to the system.

In Table 1, we give the relative positions, computed using the ATLAS *i* image, for what we take to be four components of a lensed quasar. These relative positions were used, allowing for an overall positional shift, to obtain magnitudes from the PS1 *griz* images. Natural magnitudes were computed relative to a reference star at $\alpha = 11$:34:38.15, $\delta = -21$:03:20 (with no attempt to correct for colour differences between the quasar and the PSF star). PS1 magnitudes for the reference star are given in Table 1. The measured $g-r$, $r-i$, and $r-z$ colours are consistent with quasar colours at $z_Q \sim 3.5$ (Richards et al. 2001).

The ATLAS positions were also used to obtain magnitudes from K_s images from the VISTA Hemisphere Survey (McMahon et al. 2013). As seen in Fig. 2, there is a significant residual in the K_s image, which we take to be the lensing galaxy. A second fit was carried out, allowing for a fifth point source. The relative position and magnitude for that source are included in Table 1, as are the K_s magnitudes for the four quasar images. Finally, we used all five relative positions to obtain magnitudes from the corresponding VISTA *J*-band image. The derived $J-K_s$ colour for the putative lens is consistent with that of an old stellar population at $z \sim 1$ (e.g. Bruzual & Charlot 2003).

3.2 Lens model

While the diamond-like arrangement of its four components suggests a lensed quasar, the ratio of the longer diameter to the shorter diameter is roughly 2:1, suggesting an unusually elongated gravitational potential. Among quadruply imaged quasars, only RXJ0911+0551 has a comparably elongated lensing potential.

The system was modelled using Keeton's lensmodel program.[2] The best-fitting singular isothermal ellipsoid (SIE) model had an ellipticity of 0.9, far flatter than the flattening of dark haloes in cosmological simulations. Adopting instead a singular isothermal sphere with external shear (SIS+XS), we obtain a strong shear of 0.34 at PA 43 deg E of N, and a lens strength (Einstein radius) of 1.23 arcsec. The SIS+XS model places the centre of the SIS at 0.08 arcsec from the observed position of the fifth source in the K_s image, supporting the interpretation of this object as the lensing galaxy. Table 1 gives the predicted magnification factors for the images. The observed fluxes were not used as constraints, but the predicted flux ratios are in reasonable agreement with those measured. We note in particular that the faintest image is predicted to be roughly a magnitude fainter than the other three, as observed. Also given in Table 1 are the local convergence, κ, and shear, γ, at the predicted positions, for use in microlensing applications.

Holder & Schechter (2004) have argued that quadruply imaged quasars are more often the product of external shear than of flattened haloes. The lens in the comparably sheared system RXJ0911+0551 is a member of a cluster of galaxies that provides the necessary tide. We have not been able to identify any convincing local cluster in the case of 2M1134–2103 with the presently available data, however.

4 2M1310–1714

Our second quad system, 2MASXJ13102004-1714578, hereafter 2M1310–1714, comprises a bright lens galaxy surrounded by four quasar images, again forming a 'core quad' (Fig. 1, right). Its 2MASS XSC and PS1 positions are in good accord and the PSF–Kron magnitude difference is typical for a galaxy. Hence, this discovery was purely serendipitous. In the PS1 survey, this source is deblended into five components, four of which correspond to the quasar images and one of which corresponds to the galaxy. The system has small shear, such that the quasar images fall approximately on a circle, with radius 2.9 arcsec. Interpreted as an Einstein radius θ_{Ein}, this is exceptionally large compared to other galaxy-scale quad lenses (e.g. $\langle\theta_{Ein}\rangle = 1.0$ arcsec, range 0.3–1.9 arcsec, for the sample of 12 quads modelled by Blackburne et al. 2011). Inspecting the PS1 images, we find no similarly bright galaxies in the vicinity of the 2M1310–1714, nor any clear overdensity of faint objects.

---

[1] Of the form $I(r) \propto (1 + r^2 + \frac{1}{2}\beta_4 r^4 + \frac{1}{6}\beta_6 r^6)^{-1}$; see Schechter, Mateo & Saha (1993) for details.

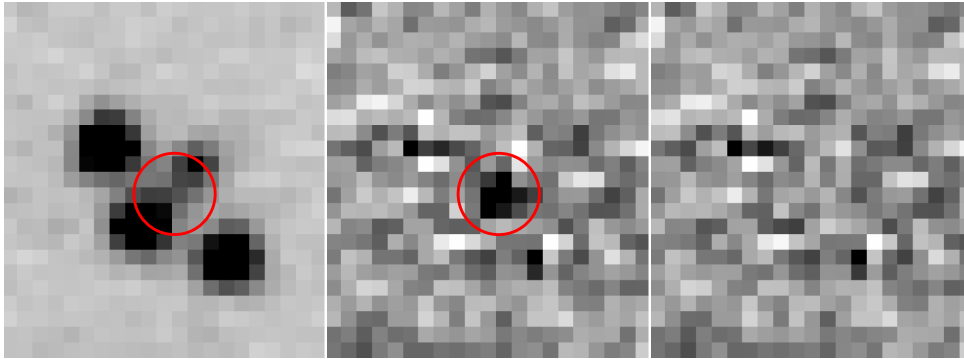[2] http://www.physics.rutgers.edu/~keeton/gravlens

Figure 2. Left: VISTA VHS K_s image of 2M1134–2103. Centre: the same image after fitting and subtracting four point sources. A significant residual peak is observed between the quasar images, which we tentatively identify as the lensing galaxy (position indicated by the red circle in first two panels). Right: residuals after fitting and subtracting five point sources. The scale is 0.34 arcsec per pixel.
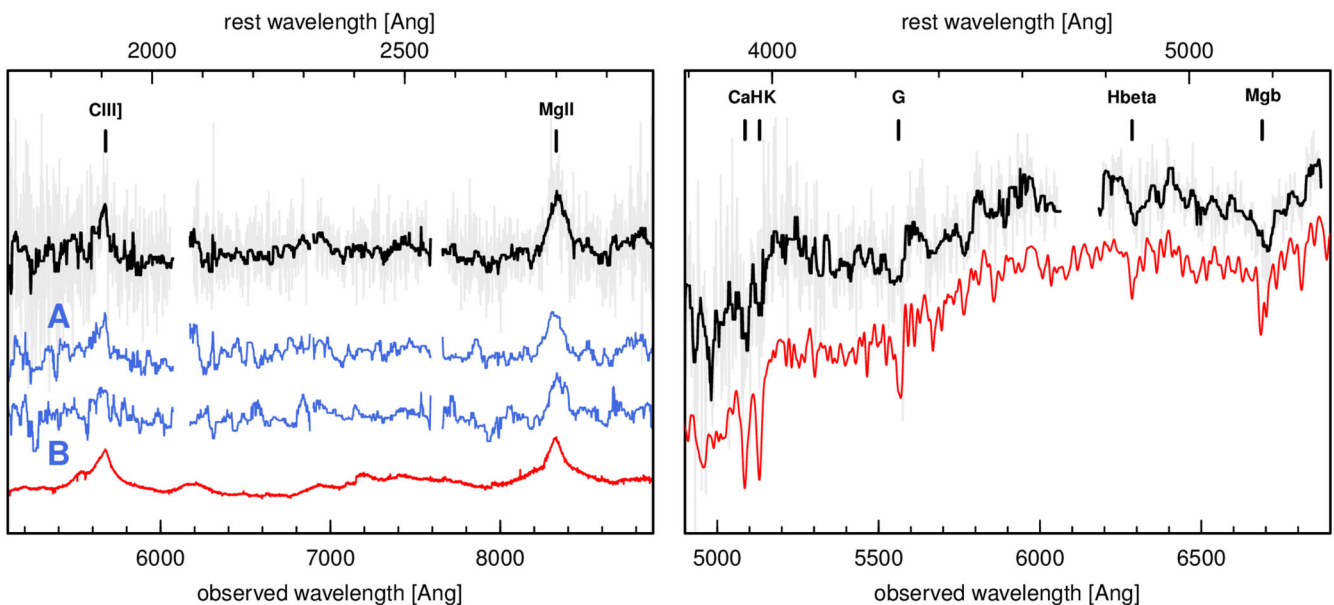

Figure 3. Left: IMACS spectrum of images *A* and *B* of the quasar in the 2M1310–1714 system. The median-smoothed spectra of the individual images are shown in blue, and the combined spectrum in black. The unsmoothed combined spectrum is shown in grey. For comparison, we show in red the Selsing et al. (2016) composite quasar spectrum, redshifted to $z_Q = 1.975$, and corresponding line identifications. Right: IMACS spectrum of the double lensing galaxy in the 2M1310–1714 system. The two components of the galaxy cannot be distinguished, and both components contribute to this spectrum. The median-smoothed spectrum is shown in black, and the unsmoothed spectrum in grey. For comparison, we show in red a composite luminous red galaxy spectrum from Dobos et al. (2012), redshifted to $z_G = 0.293$, and the corresponding line identifications.

4.1 Spectroscopy

Two long-slit spectra of 2M1310-1714 at PA 27 deg E of N were obtained with IMACS on the 6.5m Magellan Baade telescope. One of the slits passed through quasar images *A* and *B*, while the other passed through the lensing galaxies. The *f*/2 camera was used without detector binning, resulting in 0.2 arcsec pixels in the spatial direction; the spectral sampling was 1.9 Å per pixel with the 200 line/mm grism. The slit width was 0.9 arcsec. Exposures of 300 and 600 s, respectively, for the quasar and galaxy observations yielded the spectra shown in Fig. 3. The two QSO images are separated by 3 arcsec, and hence easily distinguished (the seeing was ∼0.8 arcsec FWHM). We derive a source redshift of $z_Q = 1.975$, based on the C III] and Mg II emission lines in the combined spectrum. (Only Mg II is confidently detected in the individual spectra of image *A* and *B*.) The spectrum of the galaxy has low signal-to-noise ratio, but after smoothing we confidently identify Ca II H/K lines,

the G-band and the Mg I *b* feature, placing the lens at $z_G = 0.293$. The two components of the lens galaxy cannot be distinguished with these data.

4.2 Astrometry and photometry

The central galaxy of 2M1310–1714 appears to be double in the *i* and *z* cutouts from the PS1 survey. Adopting this as a working hypothesis, we analysed the *i* cutout using our purpose-built program that simultaneously fits multiple PSFs and quasi-Gaussians to components of lensed quasar systems.

To describe this system, we fit four PSFs to the four blue images and use three additional components to represent the double lensing galaxy: two PSFs (*G1*, *G2*) with a separation of ∼1 arcsec, and an extended quasi-Gaussian capturing the extended 'halo' light from both galaxies (*H*).

Table 2. Observed and modelled parameters for the components of 2M1310–1714. The positions Δx (=$\Delta\alpha\cos\delta$), Δy (=$\Delta\delta$) are in arcsec relative to quasar image A, and were derived from the PS1 *i*-band image. The magnitudes and colours are from PS1. The final five columns provide the predicted position in our adopted lensing model (a restricted double SIE plus external shear in this case), and the predicted magnification ratio (μ, with sign indicating image parity), the local convergence (κ) and the local shear (γ). We include the predicted properties for the as-yet-unobserved fifth image E. Components G1, G2, and H represent the two point sources and one extended structure used to model the lensing galaxy pair. Source S is the reference star.

	Δx	Δy	i_{PS}	$g-r$	$r-i$	$i-z$	Δx_{mod}	Δy_{mod}	μ_{mod}	κ_{mod}	γ_{mod}
A	0.00	0.00	19.81	0.30	0.13	0.20	+0.023	+0.003	+17.2	0.477	0.464
B	−1.27	−2.61	19.89	0.20	0.13	0.16	−1.263	−2.617	−18.3	0.524	0.531
C	−3.95	+2.51	20.94	0.17	0.01	0.19	−3.942	+2.504	+16.4	0.562	0.564
D	−5.13	−2.38	19.93	0.30	0.18	0.25	−5.111	−2.364	−12.4	0.472	0.444
E							−2.960	−0.003	−0.17	3.556	3.546
G1	−2.92	−0.57	19.58	1.29	0.94	0.21					
G2	−2.98	+0.34	19.83	1.51	0.73	0.32					
H	−2.92	−0.18	17.43	1.48	0.63	0.30					
S	−29.14	−18.56	19.03	0.97	0.36	0.22					

The positions and photometry from this fit are given in Table 2. The quasi-Gaussian had major and minor axes of 3.05 and 2.25 arcsec (FWHM), respectively, with the major axis at PA −15.5 deg. The results from the *i* cutout were used to 'force' fits to the *g*, *r*, and *z* cutouts, keeping the relative positions and the shape of extended component constant but allowing the overall position and the fluxes to vary. All magnitudes were calculated relative to the PS1 magnitudes for the PSF star at $\alpha = 13{:}10{:}18.219$, $\delta = -17{:}15{:}15.99$. Colours computed from these magnitudes (again with no correction for colour difference with respect to the reference star), are given in Table 2. The combined *i*-band flux from galaxy components G1, G2, and H exceeds that from the four quasar components by a factor of 3.5.

4.3 Lens model

The double lensing galaxy in 2M1310–1714 makes mass modelling challenging. Just as it was difficult to attribute the extended light to one or the other galaxy, it is difficult to attribute the gravitational potential to one or the other. We use only the quasar image positions, as the fluxes are subject to microlensing, so the number of independent model parameters we can constrain is therefore quite limited.

We opt to describe the system with two SIEs, with their centres fixed at the positions of the two galaxy nuclei. We fix the position angles of both SIEs at the observed position angle of the halo component (PA = −15.5 deg), and set the ellipticities equal to each other, allowing them to vary in concert. The strengths of the two components are allowed to vary independently. In addition, we allowed for an external shear, but with a PA fixed at 45 deg from the PA of the SIE. Any non-zero component of shear along the PA of the SIE will be absorbed into its ellipticity, to first order. This model has six free parameters (two lens strengths, one common ellipticity, one shear component), and fits to eight constraints (positions of the four images); hence there are 2 degrees of freedom.

The derived strengths of the SIEs are 1.62 arcsec and 1.36 arcsec, respectively, for G1 and G2. The ellipticities are both 0.087, and the shear is 0.020. Table 2 includes the predicted positions, magnifications, local convergences, and local shears for the images under this model. The system is similar to PS0630–1201 (Ostrovski et al. 2018) in having double lens with a separation of roughly 1 arcsec. That system has a fifth image between the two lensing galaxies. Our model similarly predicts a fifth image, E, for 2M1310–1714, roughly five magnitudes fainter than the outer images. The pre-

dicted magnification factor for the outer images are large ($\gtrsim 15$), but are not out of line with those of other quadruply imaged quasars (cf. Blackburne et al. 2011). By contrast, models assuming a single lensing galaxy produced implausibly high magnifications ($\mu > 1000$). Fitting an alternative model with two SIS potentials, plus a free external shear, leads to a larger difference in lens strength, i.e. the centre of mass moves towards G1. This model produced larger positional residuals, for the same number of degrees of freedom.

The detection of the predicted fifth image, e.g. in future *Hubble Space Telescope* observations, would allow for refinement of our double galaxy lensing model. We also note that K_s images from the VISTA Hemisphere Survey hint at the presence of an extended Einstein ring from the quasar host, which would provide further constraints on the model; deeper observations are required to confirm and exploit this structure.

5 DISCUSSION AND SUMMARY

The two quad systems reported here were not the product of a deliberate search for lensed quasar systems. Ultimately, all Taipan galaxy targets will be visually examined. However, initially 'problem' objects were prioritized for inspection, i.e. those (i) where there is a sizeable astrometric offset (>1 arcsec) between a lower resolution 2MASS survey and a higher resolution PS1 survey and (ii) that were selected as marginally resolved 2MASS PSC sources. In addition to the quadruple systems described here, we have so far also identified 10 double point sources straddling what appears to be a lensing galaxy. Such configurations are much more likely than quads to be the result of chance projection, and hence, spectroscopic followup is essential for these cases.

Lemon et al. (2017) used differential deblending in the SDSS and *Gaia* to find lensed quasars among objects initially identified as quasars. Our technique differs in that the lens systems were initially identified as extended objects and were not selected on the basis of quasar-like colours. Our success in identifying new lenses, which were missed by other search programmes using similar survey data, suggests that our processes could be refined and converted into an effective and complementary lens discovery method.

While there are obvious biases associated with our technique, these tend to be complementary to the biases encountered with other lens discovery methods. First, the requirement that objects be extended in the 2MASS survey favours wider separation systems. By contrast, selecting for quasar-coloured objects imposes a maximum separation for the quasar components not much larger than the

resolution of the parent survey, lest they be deblended or segmented into multiple sources (Ostrovski et al. 2018). Secondly, at fixed lens and quasar redshift, the more luminous lensing galaxies are more likely to be excluded from searches for quasar-coloured objects. Our method is, by contrast, biased in favour of more luminous lensing galaxies, which also have the largest lensing cross-sections. Thirdly, *nearby* lenses are more likely to dominate the light from the lensed quasar components and are therefore more likely to be excluded from searches for quasar-coloured objects, but are favoured for selection with our approach. Nearby lenses are of particular interest because their lensing properties are less affected by dark matter, reducing an important source of systematic error in constraining the stellar initial mass function (e.g. Smith, Lucey & Conroy 2015).

The two lenses reported here resulted from a search of the Taipan region bounded by $\delta < 10$ deg and $|b| > 10$. They are both in regions covered by the VST-ATLAS survey but were not identified by Schechter et al. (2017) or Agnello et al. (2018). It would therefore seem that more quads, and many more doubles, remain to be detected using the astrometric offset technique described here. Moreover, the technique is not limited to 2MASS and Pan-STARRS. One might, for example, use SDSS and *Gaia*, as Lemon et al. (2017) have done, but look at all extended objects rather than just quasar-coloured objects.

REFERENCES

Abazajian K. N. et al., 2009, ApJS, 182, 543
Agnello A., Grillo C., Jones T., Treu T., Bonamigo M., Suyu S. H., 2017, MNRAS, 474, 3391
Agnello A. et al., 2018, MNRAS, 475, 2086
Berghea C. T., Nelson G. J., Rusu C. E., Keeton C. R., Dudik R. P., 2017, ApJ, 844, 90
Blackburne J. A., Pooley D., Rappaport S., Schechter P. L., 2011, ApJ, 729, 34
Bruzual G., Charlot S., 2003, MNRAS, 344, 1000
Chambers K. C. et al., 2016, preprint (arXiv:1612.05560)
Claeskens J.-F., Surdej J., 2002, A&AR, 10, 263
Cutri R. M. et al., 2003, CDS/ADC Collection of Electronic Catalogues, 2246
da Cunha E. et al., 2017, PASA, 34, 47
Dobos L., Csabai I., Yip C.-W., Budavári T., Wild V., Szalay A. S., 2012, MNRAS, 420, 1217
Gaia Collaboration et al., 2016, A&A, 595, A1
Holder G. P., Schechter P. L., 2003, ApJ, 589, 688
Huchra J., Gorenstein M., Kent S., Shapiro I, Smith G., Horine E., Perley R., 1985, AJ, 90, 691
Jarrett T. H., Chester T., Cutri R., Schneider S., Skrutskie M., Huchra J. P., 2000, AJ, 119, 2498
Johnston D. E. et al., 2003, AJ, 126, 2281
Lemon C. A., Auger M. W., McMahon R. G., Koposov S. E., 2017, MNRAS, 472, 5023
McGreer I. D. et al., 2010, AJ, 140, 370
McMahon R. G. et al., 2013, ESO Messenger, 154, 35
Ostrovski F. et al., 2018, MNRAS, 473, L116
Refsdal S., 1964, MNRAS, 128, 307
Richards G. T. et al., 2001, AJ, 121, 2308
Saha P., Williams L. L. R., 2003, AJ, 125, 2769
Schechter P. L., Wambsganss J., 2004, in Ryder S. D., Pisano D. J., Walker M. A., Freeman K. C., eds, Proc. IAU Symp. 220, Dark Matter in Galaxies. Sydney, Australia, p. 103
Schechter P. L., Mateo M., Saha A., 1993, PASP, 105, 1342
Schechter P. L., Pooley D., Blackburne J. A., Wambsganss J., 2014, ApJ, 793, 96
Schechter P. L., Morgan N. D., Chehade B., Metcalfe N., Shanks T., McDonald M., 2017, AJ, 153, 219
Selsing J., Fynbo J. P. U., Christensen L., Krogager J.-K., 2016, A&A, 585, A87
Shanks T. et al., 2015, MNRAS, 451, 4238
Skrutskie M. F. et al., 2006, AJ, 131, 1163
Smith R. J., Lucey J. R., Conroy C., 2015, MNRAS, 449, 3441
Treu T., Marshall P. J., 2016, A&AR, 24, 11
Wambsganss J., Paczynski B., Katz N., 1990, ApJ, 352, 407

This paper has been typeset from a TeX/LaTeX file prepared by the author.